

ARTICLE OPEN



Relative contributions of internal variability and external forcing to the inter-decadal transition of climate patterns in East Asia

Fang Huang ^{1,2}, Zhongfeng Xu ²✉, Weidong Guo ^{1,3}, Jinming Feng ², Liang Chen², Hui Zheng ² and Congbin Fu ^{1,3}

The annual precipitation in North China and South China shows a dipole pattern with a clear inter-decadal transition around the late 1970s. However, the relative contribution of internal variability and external forcing to this inter-decadal transition is still unclear. Here, we separate internal variability from the externally forced climate response through a set of dynamical downscaling simulations with lateral boundary conditions derived from reanalysis data and a large ensemble mean of the CMIP5 historical simulations. We find that internal variability accounts for about 65 and 55% of the inter-decadal transition of the annual precipitation in South and North China, respectively. By contrast, external forcing accounts for about 70% of the warming trend in eastern China over the second half of the 20th century. This study highlights the differential response of regional precipitation and air temperature to internal variability and external forcing over eastern China on an inter-decadal timescale.

npj Climate and Atmospheric Science (2023)6:21 ; <https://doi.org/10.1038/s41612-023-00351-0>

INTRODUCTION

An inter-decadal transition of the pattern of annual precipitation was observed over eastern China during the second half of the twentieth century. This transition occurred around the late 1970s and caused a long-term drying trend in North China and a wetting trend in South China, commonly referred to as the “south flood–north drought” (SFND) pattern^{1–6}. In association with this inter-decadal transition, the summer surface air temperature (SAT) also shows a cooling trend over the Yangtze River basin under the current background of global warming^{5,7,8}. Severe drought/flood disasters resulting from these anomalous precipitation patterns have major effects on water resources, agriculture, ecosystems and human society in eastern China^{9–12}. A number of factors have been identified that can affect the inter-decadal transition in the SFND pattern^{13–16}, but their relative contribution to the inter-decadal climate transition has received little attention. Understanding the causes of the inter-decadal climate transition around the late 1970s is of great importance in climate predictions on a decadal scale.

Both observational data and modeling studies suggest that the anomalous precipitation and temperature patterns in eastern China are linked to internal climate variability—that is, the Pacific decadal oscillation (PDO) and the Atlantic multi-decadal oscillation^{13,14,17,18}. The SFND pattern occurs in the PDO warm phase¹⁹. A combination of the warm phase of the PDO and the cold phase of the Atlantic multi-decadal oscillation further enhances the SFND pattern¹⁴. The abrupt increase in spring snow depth on the Tibetan Plateau after the late 1970s contributed to wetting of the Yangtze River basin^{15,20,21}. This increase in snow depth led to a decrease in the land–sea thermal contrast and weakened the Asian summer monsoon, which favored drying in North China and wetting in South China.

Many studies have argued that external forcing also affects the SFND pattern. A rapid increase in greenhouse gas concentrations

could induce a westward shift of the western North Pacific subtropical high, causing more precipitation over the Yangtze River basin²². Anthropogenic aerosols suppress convection precipitation in North China and enhance precipitation in South China^{16,23,24}. The cooling effect of anthropogenic aerosols also reduces the land–sea thermal contrast, weakening the East Asian summer monsoon and altering the distribution of rain belts in eastern China^{22,25–28}.

How much of this inter-decadal transition of precipitation over eastern China is attributable to internal variability and how much is due to external forcing remains unclear^{26,29}. Most numerical simulation studies have focused on the attribution of the inter-decadal variance in the pan-Pacific, the North Atlantic or the Northern Hemisphere^{30–33}. The attribution of the phase transition in inter-decadal variations of the Earth’s climate is hindered by the inability of coupled models to capture the observed temporal evolution of climate and the model biases in the multi-decadal variability of precipitation and temperature in East Asia^{34,35}.

Some studies have assumed that the externally forced responses are linear and independent of internal climate variability. Linear trends and generalized linear regression-based optimal fingerprint method have been widely applied to climate detection and attribution studies^{36–38}. However, the linear trends may lead to biases in the phase estimation of the internal variability^{39,40}, which is crucial in decadal climate attribution. Moreover, the optimal fingerprint method is not well applicable at the regional scale and may miss forcing factors^{41,42}. Other studies have used ensemble empirical mode decomposition (EEMD) or quadratic trends⁴² to identify the nonlinear climate response to external forcing. However, the linear and nonlinear trends are unable to represent the external forcing without a clear trend, e.g., volcanic eruptions.

Because the internal variation in individual realizations of coupled models varies independently⁴³, averaging over a large

¹School of Atmospheric Sciences, Nanjing University, Nanjing, China. ²CAS Key Laboratory of Regional Climate and Environment for Temperate East Asia, Institute of Atmospheric Physics, Chinese Academy of Sciences, 100029 Beijing, China. ³Joint International Research Laboratory of Atmospheric and Earth System Sciences, Nanjing University, Nanjing, China. ✉email: xuzhf@tea.ac.cn

number of members can greatly remove the internal variability and retain the response to changes in external forcing^{42,44–47}. The difference between the observed climate and the multi-model ensemble (MME) mean can therefore be treated as a less biased presentation of internal climate variability, especially for phase estimations^{40,48}.

To identify the response of the East Asian climate to external forcing and internal climate variability, we carried out two numerical simulations with the Weather Research and Forecasting (WRF) model during the time period 1958–2002 (see “Methods”). The first WRF simulation was driven by the ERA40 reanalysis dataset representing the joint impacts of internal variability and external forcing (the HIST simulation). The second WRF simulation was driven by the difference between the ERA40 data and the MME of 51 members from the Coupled Model Intercomparison Project Phase 5 (CMIP5) representing the impact of internal climate variability (the IV simulation). The externally forced response was represented by the historical (HIST) run minus the internal variability (IV) run, referred to here as the external forcing effect (EF). These WRF simulations can isolate the response of the regional climate to the global internal climate variability and external forcing.

RESULTS AND DISCUSSION

Observed and simulated precipitation and SAT variations in eastern China

The observed annual precipitation over eastern China (22°–43°N, 110°–122°E) shows a dipole pattern, characterized by a drying trend in the north and a wetting trend in the south (Fig. 1a). The coarse-resolution reanalysis data ERA40 (Fig. 2b), the CMIP5 MME (Fig. 2c) and a HIST experiment with 2.5° grid spacing (Supplementary Fig. 2) were unable to reproduce the

observed change in precipitation. However, the HIST experiment with 0.5° grid spacing, driven by the ERA40 reanalysis dataset, was able to successfully capture the observed dipole pattern of the precipitation (Figs. 1b and 2d), and the corresponding temporal variation (Fig. 1e, f). The ERA5 dataset, which has a finer resolution than the ERA40 dataset, can also reproduce the observed inter-decadal transition of the annual precipitation (Supplementary Fig. 3). The different performance between coarse and finer resolution simulations is likely related to their ability to resolve complex terrain. Compared with the smooth terrain in coarse resolution model, the small-scale terrain with higher elevation in finer resolution model can easily trigger convection process when large-scale circulation brings more water vapor to South China. Consequently, the finer resolution model can better capture the dipole pattern of precipitation in eastern China (Supplementary information; Supplementary Figs. 4–6). This indicates that reanalysis-driven dynamic downscaling with a higher spatial resolution is conducive to the simulation of the inter-decadal transition of the annual precipitation in eastern China. We were therefore able to quantify the relative contributions of the internal variability and external forcing to the inter-decadal climate transition in eastern China during the second half of the twentieth century based on the HIST and IV simulations.

The leading empirical orthogonal function (EOF) modes of both the HIST and IV experiments showed dipole patterns (Figs. 2d, e), which are similar to the spatial pattern of linear trends of annual precipitation (Fig. 1b, d). The WRF simulations with internal climate variability (HIST and IV) reasonably captured the temporal variation of the observed precipitation—in particular, the inter-decadal transition from a negative phase to a positive phase in the late 1970s. This indicates that the internal climate variability dominated the inter-decadal

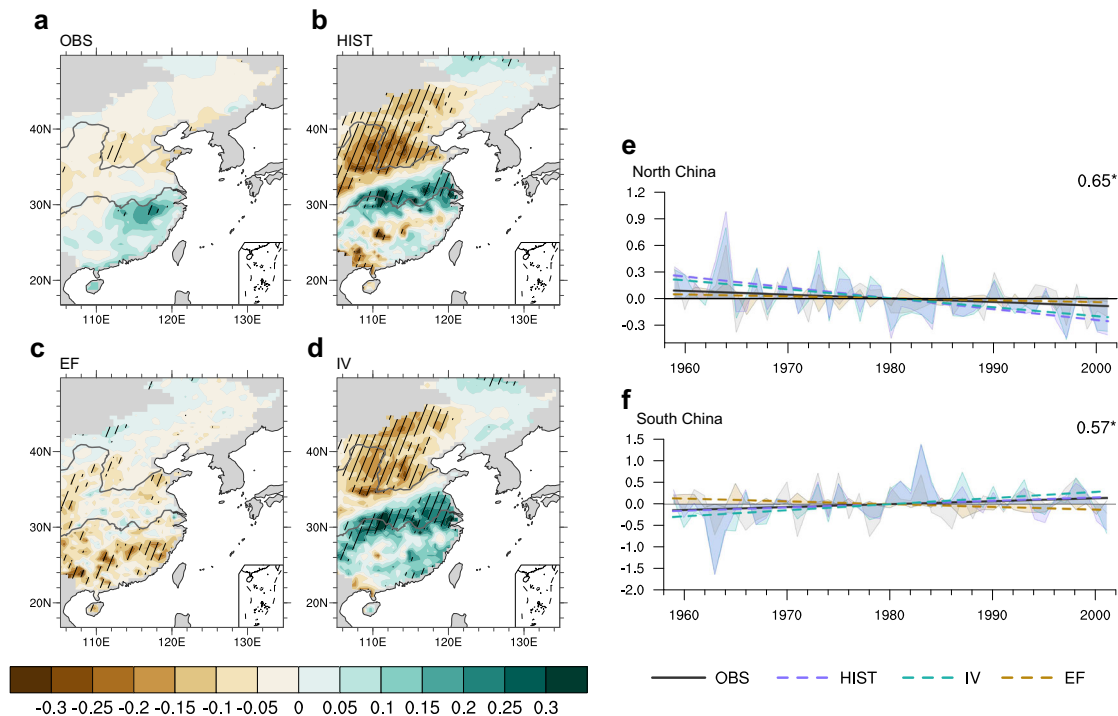


Fig. 1 Linear trends in the annual mean precipitation. Linear trends ($\text{mm day}^{-1} \text{decade}^{-1}$) in **a** observational data (CN05.1 and APHRO), **b** the WRF historical (HIST) run, **c** the response to external forcing (EF), and **d** the WRF internal variability (IV) run during the time period 1959–2001. The hatched areas and asterisks denote a significance level of 0.05. The two boxes in **a** indicating the location of North China (35°–43°N, 110°–122°E) and South China (24°–32°N, 110°–122°E). The two gray lines on the map show the location of the Yellow River in North China and the Yangtze River in central China. The time series of regional mean precipitation anomalies (shaded areas; mm day^{-1}) and the linear trends (lines; $\text{mm day}^{-1} \text{yr}^{-1}$) over **e** North China and **f** South China. The correlation coefficients between HIST and observation are shown in the upper right corner of each panel.

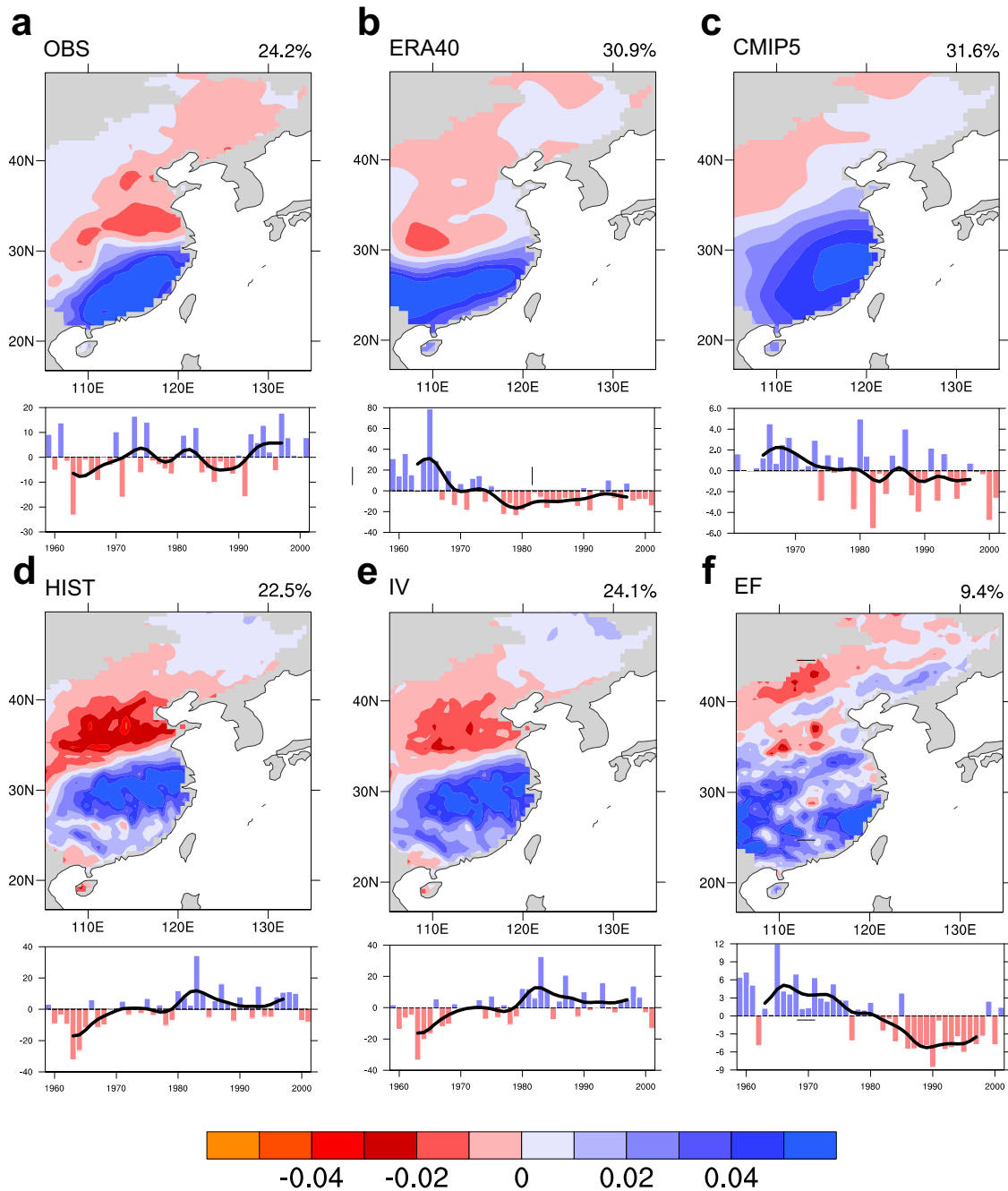


Fig. 2 Spatial patterns of the first leading empirical orthogonal functions and time series of the principal components in the annual mean precipitation during the time period 1959–2001 in eastern China. **a** Observational data (CN05.1 and APHRO), **b** ERA40 reanalysis data, **c** the MME of 17 CMIP5 models, **d** the WRF historical (HIST) run, **e** the WRF internal variability (IV) run, and **f** the response to external forcing (EF). The black thick solid lines are 9-year running mean of the principal components.

transition of the anomalous precipitation pattern over eastern China during the second half of the twentieth century. Previous studies suggested that the PDO is one of the important modes of internal variability affecting the decadal variation of precipitation in eastern China^{14,18}. The warm phase of the PDO tends to generate a cyclonic anomaly at 850-hPa over the Pacific Ocean with northwesterly wind anomalies over northern China. Consequently, the rain belt retreats to southern China and leads to a SFND pattern¹⁴. In contrast, external forcing tends to cause a drying trend over the eastern China (Fig. 1c, f). Such a drying trend can be further attributed to the increasing anthropogenic aerosol over the second half of the twentieth

century (Supplementary Fig. 10). The heavy aerosols over East Asian region can result in suppression of precipitation via the decrease in droplet radius^{49–51}. Aerosol particles act as cloud condensation nucleus to form cloud droplets. The aerosol particles compete for available water vapor. Consequently, the droplets become too small to fall as rain^{52,53}.

The observed annual mean SAT generally showed a clear warming trend over eastern China, especially in North China (Fig. 3a). The WRF simulations show high consistency with the observed SAT changes, having significant ($p < 0.05$) correlation coefficients over North China (0.86) and South China (0.64) (Fig. 3e, f). This warming pattern was also seen in the first EOF mode derived

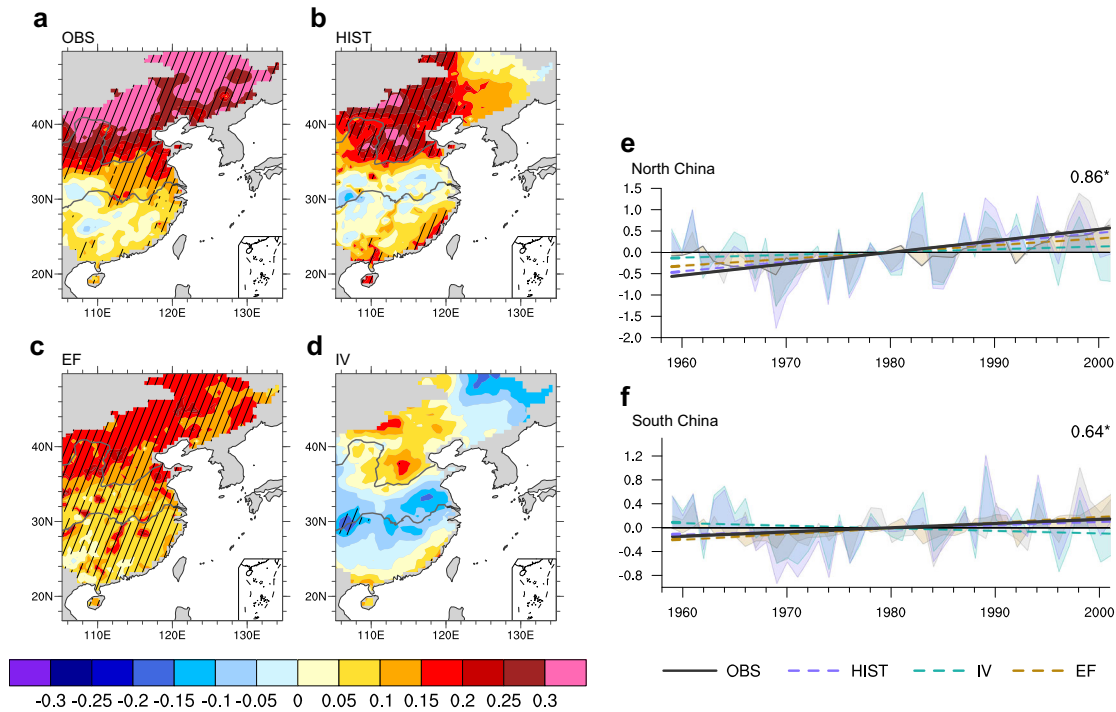


Fig. 3 Linear trends in the annual mean temperature at 2 m. Linear trends ($^{\circ}\text{C decade}^{-1}$) in **a** Observational data (CRU and UDEL), **b** the WRF historical (HIST) run, **c** the response to external forcing (EF), and **d** the WRF internal variability (IV) run during the time period 1959–2001. The hatched areas and asterisks denote a significance level of 0.05. The two gray lines on the map show the location of the Yellow River in North China and the Yangtze River in central China. The time series of regional mean temperature anomalies (shaded areas; $^{\circ}\text{C}$) and the linear trends (lines; $^{\circ}\text{C yr}^{-1}$) over **e** North China (35° – 43°N , 110° – 122°E) and **f** South China (24° – 32°N , 110° – 122°E). The correlation coefficients between HIST and observation are shown in the upper right corner of each panel.

from both the observed SAT⁵⁴ and the HIST simulation (figure not shown), with the second and third EOF modes displaying a south–north dipole and tri-pole patterns, respectively. In addition to the overall warming in eastern China, the HIST experiment also showed a slight cooling trend over the Yangtze River basin, which became clearer in the IV experiment (Fig. 3). This indicates that the cooling trend over the Yangtze River basin primarily results from the internal climate variability. Note that the decrease in the SAT was particularly significant in summer in both the HIST experiment and the observations (Supplementary Fig. 8)^{5,7,8}.

In addition to cooling over the Yangtze River basin, the IV experiment also showed a cooling trend in northeast China and a warming trend in North China (Fig. 3d). The external forcing produced a significant ($p < 0.05$) warming pattern over eastern China during the second half of the twentieth century (Fig. 3c). Comparisons among the HIST, IV and EF experiments suggested that the warming of North China resulted from both external forcing and internal variability. However, the internal variability canceled out the warming trend induced by external forcing over the Yangtze River basin and amplified the warming trend over North China. The decrease in the annual mean SAT induced by IV mainly occurs in summer (Supplementary Fig. 8) when the Yangtze River basin experiences excessive rainfall in response to the internal climate variability (Supplementary Fig. 7). The cooling (warming) trend generally corresponds to a wetting (drying) trend. An increase in precipitation is usually associated with more cloud cover, which reduces the downward solar radiation and cools the land surface. A wetter (drier) land surface tends to partition more energy into latent (sensible) heat, leading to cooling (warming) of the land surface. Synergistic changes in the SAT and precipitation over the Yangtze River basin have also been reported in previous observational and modeling studies^{5,55–57}.

Relative contributions of internal and external forcing to the dipole climate pattern

Considering that both internal variability and external forcing contribute to the inter-decadal climate transition over eastern China, we carried out a relative weight analysis (RWA)⁵⁸ based on the HIST and IV experiments to quantify their relative contributions to the annual mean precipitation and SAT. RWA is an effective approach to quantify the relative contribution among predictors of collinearity^{58–60}. Here, the RWA was applied to intrinsic mode functions (IMFs) from EEMD, which allows us to quantify the relative contribution of internal variability and external forcing to temperature or precipitation variations at different time scales.

The results showed that internal variability can explain the majority (about 85–90%) of the interannual variation in annual precipitation over eastern China (Fig. 4a). External forcing becomes more important in determining the variation of precipitation and SAT on longer timescales—for example, external forcing accounts for about 10% (35–55%) of the interannual variability (inter-decadal transition) of the annual precipitation. Notably, external forcing and internal variability make comparable contributions to the decadal variability and inter-decadal transition of precipitation in North China (Fig. 4a).

The intensified drought in North China during the last few decades is related to the weakened East Asian monsoon resulting from both the phase transition of the PDO⁶¹ and the direct effect of increased aerosols (precipitation efficiency decreases as the number and radius of cloud droplets increase)⁶². The indirect effect of anthropogenic aerosols can also suppress precipitation in North China via a reduction in droplet size⁴⁹. By contrast, the internal climate variability is more important in explaining the variations in precipitation over South China, with the proportion of variance explained ranging from about 65 to 90% on different timescales.

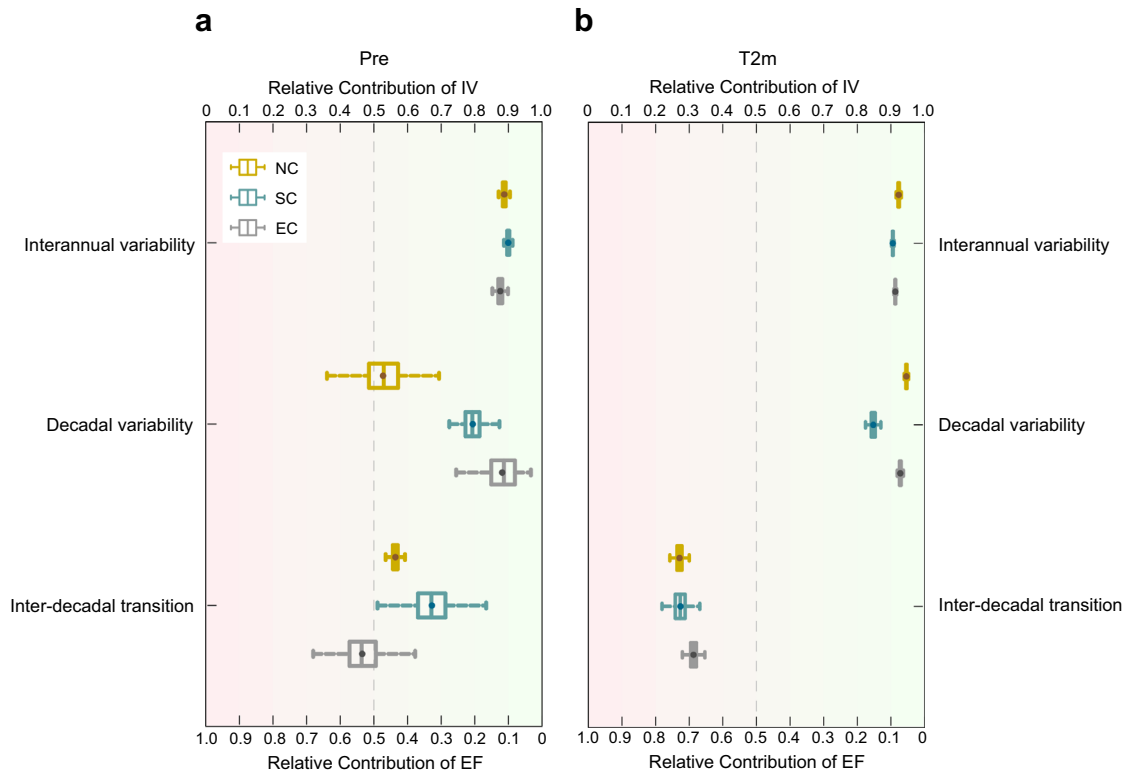


Fig. 4 Relative weight analysis of the annual mean precipitation and temperature. Relative weight analysis was applied to quantify the contributions of internal variability (IV) and external forcing (EF) to various timescales of the annual mean precipitation/temperature at 2 m over the grids in North China (NC: 35–43°N, 110–122°E; gold), South China (SC: 24–32°N, 110–122°E; green) and eastern China (EC: 22–43°N, 110–122°E; gray), respectively. Different combinations of intrinsic mode functions (IMFs) from EEMD represent the interannual variability (IMF1 + 2), decadal variability (IMF3 + 4) and nonlinear trend (IMF5), respectively. The nonlinear trend corresponds to the inter-decadal transition of **a** the annual precipitation pattern or **b** the warming trend. Bootstrap sampling with replacement was performed 1000 times on the spatial fields of the combinations of IMFs to estimate the uncertainty range of the relative weights of IV and EF. Box-plot elements: center line, median; dots, mean; box limits, upper (75th) and lower (25th) percentiles; whiskers, 1.5 times the interquartile range.

Similarly, the internal variability also dominates the interannual and decadal variation of the SAT over eastern China—for example, the internal variability accounts for about 90% of the interannual to decadal variability of the SAT in both North China and South China (Fig. 4b). By contrast, external forcing dominates the nonlinear warming trend, with an explained variance of about 70–75% over eastern China. In addition to the nonlinear warming trend, the long-term linear trend of the SAT is also dominated by external forcing (Supplementary Table 1). Compared with precipitation, SAT shows stronger response to external forcing, which is likely related to the strong long-range persistence of SAT⁴⁷.

In summary, the annual precipitation over eastern China showed an inter-decadal transition during the second half of the twentieth century, with a decrease in precipitation in North China and an increase in South China. In association with the changes in precipitation, the SAT also showed an inter-decadal variability over eastern China. Our results suggest that internal climate variability accounted for about 65% (55%) of the inter-decadal transition in anomalous precipitation in South (North) China during the second half of the twentieth century. The internal climate variability clearly dominates the inter-decadal transition in precipitation over South China. However, both the internal climate variability and external forcing have important roles in determining drying tendency in North China. In terms of the changes in the annual mean SAT, external forcing accounts for 70% of the warming trend over North China. By contrast, the internal variability dominates the cooling trend of the summer SAT over the Yangtze River basin.

Unlike previous studies that have focused on the attribution of changes in the mean climate or variance induced by various external

forcing factors, we examined the relative contribution of internal variability and time-varying external forcing to the phase transition of the inter-decadal climate variation in eastern China. We proposed a dynamical downscaling approach to separate the response of the regional climate to internal climate variability from external forcing. This study provides a novel framework for the attribution of decadal climate change that could also be applied to other regions, such as North America and northeastern Australia.

The results presented in this paper should be interpreted with caution. Firstly, we used an ensemble mean of 51 members of CMIP5 models to separate external forcing response from internal climate variability. Ensemble mean over such an ensemble size may still contain a small portion of internal climate variation, which may slightly affect the quantitative estimation of the relative contribution of internal variability and external forcing to regional climate transition over eastern China. Secondly, our WRF simulations used a simplified aerosol treatment. Although the direct and indirect effects of water- and ice-friendly aerosols were considered, the simplified treatment may still cause an inaccurate estimation of the aerosol effect to a certain degree. Lastly, we assumed the internal climate variation and external forcing are independent of each other. However, recent studies suggested that the internal climate variation (e.g. Pacific Decadal Oscillation/Inter-decadal Pacific Oscillation, Atlantic Multidecadal Oscillation) may be partly affected by external forcing (e.g., GHG and aerosols), particularly since the early 1990s^{31,32}. It remains a challenge to quantify the contribution of external forcing, through modulating PDO/IPO and AMO, to the inter-decadal climate transition in East Asia. These issues still warrant for further study.

METHODS

Data

Gauged precipitation and temperature. The observational monthly precipitation data were from the National Climate Center China CN05.1 dataset⁶³ and the Asian Precipitation–Highly-Resolved Observational Data Integration Towards the Evaluation of Water Resources (APHRODITE-MA) project of Japan⁶⁴. The CN05.1 dataset was constructed from >2400 observational stations across China and interpolated to a resolution of (0.25° × 0.25°) using the anomaly approach⁶⁵. The dataset covers the time period 1961–2014 and is widely used in studies of the impact of climate change^{66,67} and model evaluations^{68,69}. The monthly SAT data were from the gridded Climatic Research Unit Time-Series Version 4.03 (CRU TS4.03) dataset and the University of Delaware Precipitation and Air Temperature (UDEL v501) dataset.

Reanalysis and CMIP5 data. The European Centre for Medium-Range Weather Forecasts Reanalysis-40 (ERA40) dataset and the CMIP5 MME were used to generate the large-scale driving fields for the WRF model. We used historical simulations derived from 17 CMIP5 models, each with three ensemble runs. The ensemble mean was calculated using 51 historical runs (17 models × 3 ensemble runs; Table 1). The historical experiments of the CMIP5 models were forced by time-varying observed natural and anthropogenic forcing, including atmospheric greenhouse gases, solar forcing, natural and anthropogenic aerosols, and land use⁷⁰. Detailed model information can be obtained from <http://cmip-pcmdi.llnl.gov/cmip5>. In addition, ERA5 data was also used to examine the impact of model spatial resolution on the simulation of precipitation over eastern China.

Model experimental design and construction of WRF lateral boundary conditions

The ensemble mean over a large number of models can remove sufficient amounts of the internal climate variability because the internal variations among individual global climate model simulations are unrelated. The MME of the CMIP5 historical simulations therefore mainly contains the response to changes in

historical external forcing^{42,44–47}. The MME mean can better identify the forced climate response and has been used to assess various statistical methods of extracting the external forcing signal (e.g., linear trends, quadratic trends and EEMD nonlinear trends)⁴². By contrast, the reanalysis or observational data contain both internal and external forcing signals. The internal climate variability can be obtained by subtracting the MME from the observation/reanalysis data³⁹.

The ERA reanalysis data can be divided into a climatological mean plus an anomaly:

$$ERA = \overline{ERA}|_{1959-2001} + ERA' \quad (1)$$

$$ERA' = ERA'|_{FC} + ERA'|_{IV} \quad (2)$$

where $ERA'|_{FC}$ and $ERA'|_{IV}$ are the externally forced response and the internal climate variability of the reanalysis data, respectively.

The anomalous MME is:

$$MME' = MME - \overline{MME} \quad (3)$$

where \overline{MME} is the climatological mean of MME. Because the ensemble mean over a number of CMIP5 models largely cancels out the internal variabilities, the MME' is assumed to contain mainly the effect of external forcing (e.g., solar radiation, volcanic activity, greenhouse gas-induced warming trends and anthropogenic aerosols). If it is assumed that the MME can reasonably represent the temporal response of the climate to external forcing, then

$$MME' = ERA'|_{FC} \quad (4)$$

To examine the difference between the MME and the observations in representing external forcing, we calculated the nonlinear trends of the regional mean SAT derived from the MME and various observational datasets. The results indicate that the root-mean-square difference between the MME and the observations is comparable with, or even smaller than, that between various observations (Supplementary Fig. 1). This suggests that the MME approach can reasonably isolate the climate response to external forcing.

Table 1. CMIP5 models used in this study.

Model	Institution	Ensembles	
1	BCC-CSM1.1	Beijing Climate Center, China Meteorological Administration (China)	3
2	CCSM4	NCAR (National Center for Atmospheric Research) Boulder (USA)	3
3	CNRM-CM5	Centre National de Recherches Meteorologiques/Centre Europeen de Recherche et Formation Avancees en Calcul Scientifique (France)	3
4	CSIRO-Mk3-6-0	Commonwealth Scientific and Industrial Research Organization in collaboration with Queensland Climate Change Centre of Excellence (Australia)	3
5	CanESM2	Canadian Centre for Climate Modelling and Analysis (Canada)	3
6	FGOALS-g2	LASG, Institute of Atmospheric Physics, Chinese Academy of Sciences; and CESS, Tsinghua University (China)	3
7	GFDL-CM3	Geophysical Fluid Dynamics Laboratory (USA)	3
8	GISS-E2-H	NASA Goddard Institute for Space Studies (USA)	3
9	GISS-E2-R	NASA Goddard Institute for Space Studies (USA)	3
10	HadCM3	Met Office Hadley Centre (England)	3
11	IPSL-CM5A-LR	Institute Pierre-Simon Laplace (France)	3
12	MIROC-ESM	Japan Agency for Marine-Earth Science and Technology, Atmosphere and Ocean Research Institute (The University of Tokyo), and National Institute for Environmental Studies (Japan)	3
13	MIROC5	Atmosphere and Ocean Research Institute (The University of Tokyo), National Institute for Environmental Studies, and Japan Agency for Marine-Earth Science and Technology (Japan)	3
14	MPI-ESM-LR	Max Planck Institute for Meteorology (Germany)	3
15	MPI-ESM-MR	Max Planck Institute for Meteorology (Germany)	3
16	MRI-CGCM3	Meteorological Research Institute (Japan)	3
17	NorESM1-M	Norwegian Climate Centre (Norway)	3

Table 2. WRF model attribution experiments.

Experiment	External forcing in WRF model	External forcing in the lateral boundary conditions
HIST	Time-varying external forcings, including greenhouse gas concentrations, anthropogenic aerosols, ozone, land use and land cover change, volcanic aerosols, solar insolation	ERA40
IV	Climatological mean external forcings, including greenhouse gas concentrations, anthropogenic aerosols, ozone, land use and land cover change, volcanic aerosols, solar insolation	ERA40 – MME'

We use the ERA reanalysis data as the lateral boundary conditions (LBCs) of the historical (HIST) experiment:

$$\begin{aligned} \text{LBC}|_{\text{HIST}} &= \text{ERA} \\ &= \overline{\text{ERA}}|_{1959-2001} + \text{ERA}' \\ &= \overline{\text{ERA}}|_{1959-2001} + \text{ERA}'|_{\text{FC}} + \text{ERA}'|_{\text{IV}} \end{aligned} \quad (5)$$

Using Eqs. (1–4), we constructed the LBCs for the internal variability (IV) experiment:

$$\begin{aligned} \text{LBC}|_{\text{IV}} &= \overline{\text{ERA}}|_{1959-2001} + \text{ERA}'|_{\text{IV}} \\ &= \overline{\text{ERA}}|_{1959-2001} + \text{ERA}' - \text{ERA}'|_{\text{FC}} \\ &= \overline{\text{ERA}}|_{1959-2001} + \text{ERA}' - \text{MME}' \\ &= \text{ERA} - \text{MME}' \end{aligned} \quad (6)$$

Note that, similar to Eq. (5), the LBCs in Eq. (6) have a reanalysis-based mean climate, which removes the mean bias in the MME and generates more reliable dynamical downscaling simulations for the historical climate.

We carried out two sets of WRF simulations (HIST and IV) driven by the large-scale forcing variables, including SST, surface pressure, sea level pressure, air temperature, zonal wind, meridional wind, relative humidity, and geopotential height, constructed in Eqs. (5) and (6), respectively (Table 2). In the HIST experiment, the WRF simulations considered the observed transient variation of natural and anthropogenic external forcing factors (e.g., solar radiation, volcanic aerosols, ozone, greenhouse gases, anthropogenic aerosols, and changes in land use and land cover; see Supplementary Information). In the IV experiment, the natural and external forcings were fixed at their climatological mean to remove the temporal variation of external forcing. The HIST experiment considered the time-varying external forcing and internal climate variability in both the WRF inner domain and its LBCs. By contrast, the IV experiment considered the internal variability only and held the external forcing factors at their climatological means in the WRF model and the external forcings were removed from its LBCs. Both the LBCs of the HIST and IV experiment inherit the internal climate variability from the ERA40 reanalysis.

The effect of external forcing can be represented by the difference between the HIST and IV experiments (HIST – IV), which isolates the climate response to external forcing under realistic internal climate variability. The HIST – IV and CMIP5 MME show comparable temporal variation in eastern China, which gives us more confidence to use the HIST – IV representing external forcing effect (Supplementary Fig. 11).

Relative weight analysis

We used Johnson's relative weight analysis (RWA)⁵⁸ to quantify the relative importance of internal variability (IV) and external forcing (EF). RWA addresses the problem of collinearity among predictors in the attribution based on multivariate linear regression^{59,60}. It first creates a new set of uncorrelated predictors $Z(z_k)$ by orthogonally transforming the original set of predictors $X(x_j)$. Two regression analyses are then conducted using the orthogonal predictors: one

generates the standardized regression coefficient β by regressing the dependent variable Y on Z . Another generates the standardized regression coefficient λ by regressing the original predictor X on Z . The relative contribution of the original variable X to the dependent variable Y is then obtained through combining β with λ :

$$\varepsilon_j = \sum_{k=1}^p \lambda_{jk}^2 \beta_k^2 \quad (7)$$

where ε_j is the relative importance of predictor j , which is IV or EF in this study. β_k^2 and λ_{jk}^2 are the squares of the standardized regression coefficients linking orthogonal predictor k with the dependent variable and original predictor j , respectively. The actual relative contributions of IV and EF are quantified as $\frac{\varepsilon_{\text{IV}}}{\varepsilon_{\text{IV}} + \varepsilon_{\text{EF}}}$ and $\frac{\varepsilon_{\text{EF}}}{\varepsilon_{\text{IV}} + \varepsilon_{\text{EF}}}$, respectively. The RWA method was successfully applied to the quantification of the relative contributions of different external drivers and internal variability to regional changes in temperature⁷¹, the relative contribution rate of meteorological and land use factors to a reduction in surface runoff⁷² and the biophysical and socioeconomic drivers of changes in forest and agricultural land⁷³.

RWA was performed on different combinations of the intrinsic mode functions (IMFs) of the ensemble empirical mode decomposition in the annual mean precipitation and surface air temperature. Different combinations of IMFs represent the information in various timescales of climate variations^{74–76}. We obtained four IMFs and the residual based on the ensemble empirical mode decomposition of the 43-year time series from 1959 to 2001. The first and second IMFs are of high-frequency oscillation signals on timescale <10 years, representing internal variability. The third and fourth IMFs are decadal oscillation signals with timescales >10 years. The residual component is a nonlinear trend that describe the inter-decadal transition in the second half of the twentieth century (Supplementary Figs. 12 and 13). Bootstrap sampling with replacement was performed 1000 times on the spatial fields of different combinations of IMFs to estimate the uncertainty range of the RWA analysis of the IV and EF effects.

DATA AVAILABILITY

The original CMIP5 database can be downloaded from the Earth System Grid Federation (ESGF) server (<https://esgf-node.llnl.gov/projects/cmip5/>). The ERA40 and ERA5 data were obtained from the European Center for Medium-Range Weather Forecast (<https://www.ecmwf.int/en/forecasts/datasets>). The CN05.1 data was downloaded from <http://data.cma.cn/>. The APHRODITE-MA data were downloaded from http://search.diasjp.net/en/dataset/APHRO_MA. The CRU data were downloaded from <https://crudata.uea.ac.uk/cru/data/hrg/>. The UDEL data were obtained from the NOAA web https://psl.noaa.gov/data/gridded/data.UDel_AirT_Precip.html. Derived data supporting the findings of this study are available from the corresponding author upon reasonable request.

CODE AVAILABILITY

Codes are available upon reasonable request from the corresponding author.

Received: 22 April 2022; Accepted: 9 March 2023;
Published online: 23 March 2023

REFERENCES

- Weng, H., Lau, K. M. & Xue, Y. Multi-scale summer rainfall variability over China and its long-term link to global sea surface temperature variability. *J. Meteorol. Soc. Jpn. Ser. II* **77**, 845–857 (1999).
- Chang, C. P., Zhang, Y. & Li, T. Interannual and interdecadal variations of the East Asian summer monsoon and tropical Pacific SSTs. Part II: Meridional structure of the monsoon. *J. Clim.* **13**, 4326–4340 (2000).
- Ding, Y., Wang, Z. & Sun, Y. Inter-decadal variation of the summer precipitation in East China and its association with decreasing Asian summer monsoon. Part I: Observed evidences. *Int. J. Climatol.* **28**, 1139–1161 (2008).
- Hu, Z.-Z. Long-term climate variations in China and global warming signals. *J. Geophys. Res.* <https://doi.org/10.1029/2003jd003651> (2003).
- Qian, W. & Lin, X. Regional trends in recent temperature indices in China. *Clim. Res.* **27**, 119–134 (2004).
- Zhou, T. & Yu, R. Twentieth-century surface air temperature over China and the globe simulated by coupled climate models. *J. Clim.* **19**, 5843–5858 (2006).
- Yatagai, A. & Yasunari, T. Trends and decadal-scale fluctuations of surface air temperature and precipitation over China and Mongolia during the recent 40 year period (1951–1990). *J. Meteorol. Soc. Jpn. Ser. II* **72**, 937–957 (1994).
- Guan, Y., Zhang, X., Zheng, F. & Wang, B. Trends and variability of daily temperature extremes during 1960–2012 in the Yangtze River Basin, China. *Glob. Planet. Change* **124**, 79–94 (2015).
- Ma, Z. & Fu, C. Some evidence of drying trend over northern China from 1951 to 2004. *Chin. Sci. Bull.* **51**, 2913–2925 (2006).
- Gong, D.-Y. & Ho, C.-H. Shift in the summer rainfall over the Yangtze River valley in the late 1970s. *Geophys. Res. Lett.* **29**, 78–71–78–74 (2002).
- Wang, A. H., Lettenmaier, D. P. & Sheffield, J. Soil moisture drought in China, 1950–2006. *J. Clim.* **24**, 3257–3271 (2011).
- Ma, S., Zhou, T., Dai, A. & Han, Z. Observed changes in the distributions of daily precipitation frequency and amount over China from 1960 to 2013. *J. Clim.* **28**, 6960–6978 (2015).
- Zhang, L. & Zhou, T. Drought over East Asia: a review. *J. Clim.* **28**, 3375–3399 (2015).
- Yang, Q. et al. Decadal modulation of precipitation patterns over Eastern China by sea surface temperature anomalies. *J. Clim.* **30**, 7017–7033 (2017).
- Ding, Y., Sun, Y., Wang, Z., Zhu, Y. & Song, Y. Inter-decadal variation of the summer precipitation in China and its association with decreasing Asian summer monsoon Part II: Possible causes. *Int. J. Climatol.* **29**, 1926–1944 (2009).
- Yu, S. et al. Anthropogenic aerosols are a potential cause for migration of the summer monsoon rain belt in China. *Proc. Natl Acad. Sci. USA* **113**, E2209–E2210 (2016).
- Zhu, Y., Wang, H., Zhou, W. & Ma, J. Recent changes in the summer precipitation pattern in East China and the background circulation. *Clim. Dyn.* **36**, 1463–1473 (2010).
- Zhang, Z., Sun, X. & Yang, X.-Q. Understanding the interdecadal variability of East Asian summer monsoon precipitation: joint influence of three oceanic signals. *J. Clim.* **31**, 5485–5506 (2018).
- Zhu, Y., Wang, T. & Ma, J. Influence of internal decadal variability on the summer rainfall in Eastern China as simulated by CCSM4. *Adv. Atmos. Sci.* **33**, 706–714 (2016).
- Zhang, Y., Li, T. & Wang, B. Decadal change of the spring snow depth over the Tibetan Plateau: the associated circulation and influence on the East Asian summer monsoon. *J. Clim.* **17**, 2780–2793 (2004).
- Wu, T. & Qian, Z. The relation between the Tibetan winter snow and the Asian summer monsoon and rainfall: an observational investigation. *J. Clim.* **16**, 2038–2051 (2003).
- Wang, T. et al. Anthropogenic agent implicated as a prime driver of shift in precipitation in eastern China in the late 1970s. *Atmos. Chem. Phys.* **13**, 12433–12450 (2013).
- Jiang, Y., Liu, X., Yang, X.-Q. & Wang, M. A numerical study of the effect of different aerosol types on East Asian summer clouds and precipitation. *Atmos. Environ.* **70**, 51–63 (2013).
- Li, Z. et al. Suppression of convective precipitation by elevated man-made aerosols is responsible for large-scale droughts in north China. *Proc. Natl Acad. Sci. USA* **115**, E8327–E8328 (2018).
- Song, F., Zhou, T. & Qian, Y. Responses of East Asian summer monsoon to natural and anthropogenic forcings in the 17 latest CMIP5 models. *Geophys. Res. Lett.* **41**, 596–603 (2014).
- Zhou, T., Gong, D., Li, J. & Li, B. Detecting and understanding the multi-decadal variability of the East Asian summer monsoon: recent progress and state of affairs. *Meteorol. Z.* **18**, 455–467 (2009).
- Dong, B., Wilcox, L. J., Highwood, E. J. & Sutton, R. T. Impacts of recent decadal changes in Asian aerosols on the East Asian summer monsoon: roles of aerosol–radiation and aerosol–cloud interactions. *Clim. Dyn.* **53**, 3235–3256 (2019).
- Twomey, S. Influence of pollution on shortwave Albedo of clouds. *J. Atmos. Sci.* **34**, 1149–1152 (1977).
- Wang, B. et al. Monsoons climate change assessment. *Bull. Am. Meteorol. Soc.* **102**, E1–E19 (2021).
- Steinman, B. A., Mann, M. E. & Miller, S. K. Climate change. Atlantic and Pacific multidecadal oscillations and Northern Hemisphere temperatures. *Science* **347**, 988–991 (2015).
- Hua, W., Dai, A. & Qin, M. Contributions of internal variability and external forcing to the recent Pacific decadal variations. *Geophys. Res. Lett.* **45**, 7084–7092 (2018).
- Qin, M., Dai, A. & Hua, W. Aerosol-forced multidecadal variations across all ocean basins in models and observations since 1920. *Sci. Adv.* <https://doi.org/10.1126/sciadv.abb0425> (2020).
- Qin, M., Dai, A. & Hua, W. Quantifying contributions of internal variability and external forcing to Atlantic multidecadal variability since 1870. *Geophys. Res. Lett.* <https://doi.org/10.1029/2020gl089504> (2020).
- Chen, L. & Frauenfeld, O. W. A comprehensive evaluation of precipitation simulations over China based on CMIP5 multimodel ensemble projections. *J. Geophys. Res. Atmos.* **119**, 5767–5786 (2014).
- Chen, L. & Frauenfeld, O. W. Surface air temperature changes over the twentieth and twenty-first centuries in China simulated by 20 CMIP5 models. *J. Clim.* **27**, 3920–3937 (2014).
- Zhang, X. et al. Detection of human influence on twentieth-century precipitation trends. *Nature* **448**, 461–465 (2007).
- Swart, N. C., Gille, S. T., Fyfe, J. C. & Gillett, N. P. Recent Southern Ocean warming and freshening driven by greenhouse gas emissions and ozone depletion. *Nat. Geosci.* **11**, 836–841 (2018).
- Najafi, M. R., Zwiers, F. W. & Gillett, N. P. Attribution of Arctic temperature change to greenhouse-gas and aerosol influences. *Nat. Clim. Change* **5**, 246–249 (2015).
- Mann, M. E., Steinman, B. A. & Miller, S. K. On forced temperature changes, internal variability, and the AMO. *Geophys. Res. Lett.* **41**, 3211–3219 (2014).
- Frankcombe, L. M., England, M. H., Mann, M. E. & Steinman, B. A. Separating internal variability from the externally forced climate response. *J. Clim.* **28**, 8184–8202 (2015).
- Zwiers, F. W. & Zhang, X. Toward regional-scale climate change detection. *J. Clim.* **16**, 793–797 (2003).
- Frankignoul, C., Gastineau, G. & Kwon, Y.-O. Estimation of the SST response to anthropogenic and external forcing and its impact on the Atlantic multidecadal oscillation and the Pacific decadal oscillation. *J. Clim.* **30**, 9871–9895 (2017).
- Taylor, K. E., Stouffer, R. J. & Meehl, G. A. An overview of CMIP5 and the experiment design. *Bull. Am. Meteorol. Soc.* **93**, 485–498 (2012).
- Dai, A., Fyfe, J. C., Xie, S.-P. & Dai, X. Decadal modulation of global surface temperature by internal climate variability. *Nat. Clim. Change* **5**, 555–559 (2015).
- Huang, X. et al. The recent decline and recovery of Indian summer monsoon rainfall: relative roles of external forcing and internal variability. *J. Clim.* **33**, 5035–5060 (2020).
- Liguori, G., McGregor, S., Arblaster, J. M., Singh, M. S. & Meehl, G. A. A joint role for forced and internally-driven variability in the decadal modulation of global warming. *Nat. Commun.* **11**, 3827 (2020).
- Li, Q. et al. Different climate response persistence causes warming trend unevenness at continental scales. *Nat. Clim. Change* <https://doi.org/10.1038/s41558-022-01313-9> (2022).
- Luo, M. et al. Decadal wintertime temperature changes in East Asia during 1958–2001 and the contributions of internal variability and external forcing. *J. Geophys. Res. Atmos.* <https://doi.org/10.1029/2019jd031840> (2020).
- Qian, Y. et al. Heavy pollution suppresses light rain in China: Observations and modeling. *J. Geophys. Res.* <https://doi.org/10.1029/2008jd011575> (2009).
- Cheng, Y. J., Lohmann, U. & Zhang, J. H. Contribution of changes in sea surface temperature and aerosol loading to the decreasing precipitation trend in Southern China. *J. Clim.* **18**, 1381–1390 (2005).
- Sun, N., Fu, Y. F., Zhong, L. & Li, R. Aerosol effects on the vertical structure of precipitation in East China. *npj Clim. Atmos. Sci.* <https://doi.org/10.1038/s41612-022-00284-0> (2022).
- Rosenfeld, D. Suppression of rain and snow by urban and industrial air pollution. *Science* **287**, 1793–1796 (2000).
- Ramanathan, V., Crutzen, P. J., Kiehl, J. T. & Rosenfeld, D. Aerosols, climate, and the hydrological cycle. *Science* **294**, 2119–2124 (2001).
- Liu, Z. et al. Evaluation of spatial and temporal performances of ERA-interim precipitation and temperature in Mainland China. *J. Clim.* **31**, 4347–4365 (2018).
- Wu, R., Chen, J. & Wen, Z. Precipitation–surface temperature relationship in the IPCC CMIP5 models. *Adv. Atmos. Sci.* **30**, 766–778 (2013).
- Li, Q. et al. China experiencing the recent warming hiatus. *Geophys. Res. Lett.* **42**, 889–898 (2015).

57. Hu, K., Huang, G. & Xie, S.-P. Assessing the internal variability in multi-decadal trends of summer surface air temperature over East Asia with a large ensemble of GCM simulations. *Clim. Dyn.* **52**, 6229–6242 (2018).
58. Johnson, J. W. A heuristic method for estimating the relative weight of predictor variables in multiple regression. *Multivar. Behav. Res.* **35**, 1–19 (2000).
59. Tonidandel, S., LeBreton, J. M. & Johnson, J. W. Determining the statistical significance of relative weights. *Psychol. Methods* **14**, 387–399 (2009).
60. Tonidandel, S. & LeBreton, J. M. Relative importance analysis: a useful supplement to regression analysis. *J. Bus. Psychol.* **26**, 1–9 (2011).
61. Qian, C. & Zhou, T. Multidecadal variability of North China aridity and its relationship to PDO during 1900–2010. *J. Clim.* **27**, 1210–1222 (2014).
62. Zhang, L., Peili, W. & Zhou, T. Aerosol forcing of extreme summer drought over North China. *Environ. Res. Lett.* **12**, 034020 (2017).
63. Wu, J. & Gao, X. A gridded daily observation dataset over China region and comparison with the other datasets. *Chin. J. Geophys.* **56**, 1102–1111 (2013).
64. Yatagai, A. et al. APHRODITE: constructing a long-term daily gridded precipitation dataset for Asia based on a dense network of rain gauges. *Bull. Am. Meteorol. Soc.* **93**, 1401–1415 (2012).
65. New, M., Hulme, M. & Jones, P. Representing twentieth-century space–time climate variability. Part II: Development of 1901–96 monthly grids of terrestrial surface climate. *J. Clim.* **13**, 2217–2238 (2000).
66. He, S., Gao, Y., Li, F., Wang, H. & He, Y. Impact of Arctic oscillation on the East Asian climate: a review. *Earth Sci. Rev.* **164**, 48–62 (2017).
67. Wang, J. et al. Recent global decline in endorheic basin water storages. *Nat. Geosci.* **11**, 926–932 (2018).
68. Yang, Y., Tang, J., Xiong, Z. & Dong, X. Evaluation of high-resolution gridded precipitation data in arid and semiarid regions: Heihe River Basin, Northwest China. *J. Hydrometeorol.* **18**, 3075–3101 (2017).
69. Zhou, B., Wen, Q. H., Xu, Y., Song, L. & Zhang, X. Projected changes in temperature and precipitation extremes in China by the CMIP5 multimodel ensembles. *J. Clim.* **27**, 6591–6611 (2014).
70. Taylor, K. E., Stouffer, R. J. & Meehl, G. A. A summary of the CMIP5 experiment design. PCMDI Reports. https://pcmdi.llnl.gov/mips/cmip5/docs/Taylor_CMIP5_22Jan11_marked.pdf (2009).
71. Song, M., Wang, R., Ljungqvist, F. C., Wang, X. & Yang, T. Winter vs. summer temperature variations on the southeastern Tibetan Plateau, 1718–2005 CE. *Atmos. Res.* <https://doi.org/10.1016/j.atmosres.2021.105739> (2021).
72. Li, R. et al. Time and space catch up with restoration programs that ignore ecosystem service trade-offs. *Sci. Adv.* **7**, eabf8650 (2021).
73. Xu, X., Jain, A. K. & Calvin, K. V. Quantifying the biophysical and socioeconomic drivers of changes in forest and agricultural land in South and Southeast Asia. *Glob. Chang. Biol.* **25**, 2137–2151 (2019).
74. McMahon, T. A., Kiem, A. S., Peel, M. C., Jordan, P. W. & Pegram, G. G. S. A new approach to stochastically generating six-monthly rainfall sequences based on empirical mode decomposition. *J. Hydrometeorol.* **9**, 1377–1389 (2008).
75. Gao, L. H., Yan, Z. W. & Quan, X. W. Observed and SST-forced multidecadal variability in global land surface air temperature. *Clim. Dyn.* **44**, 359–369 (2014).
76. Rajesh, P. V. & Goswami, B. N. Four-dimensional structure and sub-seasonal regulation of the Indian summer monsoon multi-decadal mode. *Clim. Dyn.* **55**, 2645–2666 (2020).

ACKNOWLEDGEMENTS

This study was supported jointly by the National Key R&D Program of China (No. 2022YFF0802503; No. 2016YFA0600403), the National Science Foundation of China (No. 42075170; No. 42130602) and the Jiangsu Collaborative Innovation Center for Climate Change. We acknowledge the World Climate Research Programme’s Working Group on Coupled Modelling, which is responsible for the CMIP, and thank the climate modeling groups for producing the model output and making it available.

AUTHOR CONTRIBUTIONS

Z.X. designed the study and conducted the experiments. F.H. carried out the data analysis and coarse resolution WRF simulation. F.H. and Z.X. led the writing of the paper. J.F. and L.C. modified the Weather Research and Forecasting code to incorporate external forcing. H.Z. prepared the land cover data. All authors discussed the results and edited and commented on the manuscript.

COMPETING INTERESTS

The authors declare no competing interests.

ADDITIONAL INFORMATION

Supplementary information The online version contains supplementary material available at <https://doi.org/10.1038/s41612-023-00351-0>.

Correspondence and requests for materials should be addressed to Zhongfeng Xu.

Reprints and permission information is available at <http://www.nature.com/reprints>

Publisher’s note Springer Nature remains neutral with regard to jurisdictional claims in published maps and institutional affiliations.



Open Access This article is licensed under a Creative Commons Attribution 4.0 International License, which permits use, sharing, adaptation, distribution and reproduction in any medium or format, as long as you give appropriate credit to the original author(s) and the source, provide a link to the Creative Commons license, and indicate if changes were made. The images or other third party material in this article are included in the article’s Creative Commons license, unless indicated otherwise in a credit line to the material. If material is not included in the article’s Creative Commons license and your intended use is not permitted by statutory regulation or exceeds the permitted use, you will need to obtain permission directly from the copyright holder. To view a copy of this license, visit <http://creativecommons.org/licenses/by/4.0/>.

© The Author(s) 2023